

Lidar-only Odometry based on Multiple Scan-to-Scan Alignments over a Moving Window

Aaron Kurda, Simon Steuernagel, and Marcus Baum

Abstract—Lidar-only odometry considers the pose estimation of a mobile robot based on the accumulation of motion increments extracted from consecutive lidar scans. Many existing approaches to the problem use a scan-to-map registration, which neglects the accumulation of errors within the maintained map due to drift. Other methods use a refinement step that jointly optimizes the local map on a feature basis. We propose a solution that avoids this by using multiple independent scan-to-scan Iterative Closest Points (ICP) registrations to previous scans in order to derive constraints for a pose graph. The optimization of the pose graph then not only yields an accurate estimate for the latest pose, but also enables the refinement of previous scans in the optimization window. By avoiding the need to recompute the scan-to-scan alignments, the computational load is minimized. Extensive evaluation on the public KITTI and MulRan datasets as well as on a custom automotive lidar dataset is carried out. Results show that the proposed approach achieves state-of-the-art estimation accuracy, while alleviating the mentioned issues.

I. INTRODUCTION

Odometry is the task of estimating the movement of a mobile platform w.r.t. a given starting position and is therefore a prerequisite for many other tasks. The ability of lidar sensors to sense their environment make them particularly interesting as their measurement can be used for mapping [1]. This makes lidar odometry especially suitable for robots that aim at navigating space autonomously. The general idea behind lidar odometry is to infer the motion of a mobile platform relative to its (static) environment by aligning the measurements of the sensor over a short period of time. A common choice of algorithm for this alignment is the ICP [2] algorithm, which takes two point clouds, i.e., lidar scans, and finds the transformation that best aligns them. This process is also called registration and its solution provides an estimate of the motion between the two recordings. To infer the motion over longer periods, a simple solution is to recursively apply the registration method to consecutive pairs of lidar scans [3]. The resulting list of motion estimates then describe the traversed path of the agent (Fig. 1a). The recursive estimation of the pose from the motion is also called dead reckoning and is widely used in inertial odometry using, e.g., Inertial Measurement Unit (IMU) sensors. Its key problem is that the errors of individual registrations accumulate over time, resulting in a drifting estimate of the traversed path. Many

This work was funded by the German Federal Ministry for Economic Affairs and Climate Action (BMWK) within the research project “OKULAr” (Grant No. 19A22003C).

The authors are with the Institute of Computer Science, University of Goettingen, Goettingen, Germany.

E-mail: {aaron.kurda, simon.steuernagel, marcus.baum}@cs.uni-goettingen.de

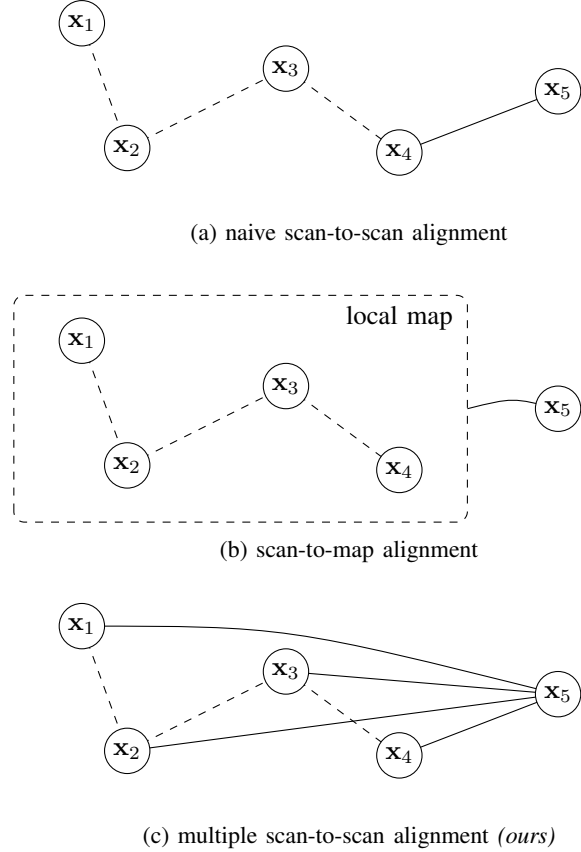


Fig. 1: Schematic representation of (a): naive scan-to-scan (b): scan-to-map and (c): *our* proposed registration method for the estimation of the current pose x_5 . Dashed lines indicate motion constraints from previous time steps.

modern methods utilize a *local map* approach, where a new lidar scan is registered against an accumulation of previously aligned lidar scans [4] (Fig. 1b). While this idea has been proven to reduce the accumulation of drift over the naive approach, it also introduces (additional) correlations between the registrations. Where the result of the scan-to-scan method only depends on the two input scans (and optionally a motion prediction), the outcome of a registration in the scan-to-map approach further depends on the correctness of the map and therefore correlates with the previous registrations.

In recent years, the idea of Smoothing and Mapping (SAM) [5] has taken hold in the lidar odometry community. Here, in contrast to the aforementioned filtering approaches, a retrospective update of previous poses is carried out, which

generally increases estimation quality. Smoothing can be implemented by jointly optimizing multiple lidar scans in a local window on a feature-level [6], [7]. This, however, is expensive in computation time and therefore might not be applicable for every time step. Another approach is to derive motion constraints from the registration of lidar scans and use pose graph optimization to find a configuration of nodes that best satisfies these constraints. Conventional lidar odometry methods do not natively benefit from this, as their registration essentially forms a linked list of nodes connected via constraints. The addition of further constraints by integration of sensor measurements like IMU or Global Navigation Satellite System (GNSS) is a common approach to solve this problem, which, however, requires the use of additional hardware [8]. An alternative to this is to derive multiple constraints from lidar odometry directly through the use of multiple registrations [9], [10]. Here, a new lidar scan is aligned against a set of previous lidar scans. The resulting set of constraints can then, together with the constraints from previous time steps, be used for a pose graph optimization. These approaches however are mainly used in *full* Simultaneous Localization and Mapping (SLAM) problems, with the aim at producing a coherent map and not as lidar odometry approaches.

A. Contribution

In this paper we present a simple lidar-only SAM approach to lidar odometry that offers real-time filtering as well as lagged smoothing capabilities. We avoid the use of feature-based joint optimization through the use of multiple independent scan-to-scan registrations against a set of previous lidar scans (Fig. 1c). Optimizing these newly established constraints together with constraints from previous time steps results in an accurate pose estimate for the current time step as well as a set of consistent previous poses. The core of our method is an adaption of the well-known ICP algorithm proposed in [4]. We evaluate the method on KITTI [11], MulRan [12] as well as on our custom dataset and compare the results against other state-of-the-art methods. Results show an increased accuracy on the majority of the sequences of the MulRan and our custom data dataset, and comparable results to other state-of-the-art methods on the KITTI dataset, proving its effectiveness in automotive settings.

II. RELATED WORK

Lidar odometry can at its core be interpreted as a combined registration and data management problem. While different registration methods have been proposed in the past [13], most modern lidar odometry approaches utilize a version of the ICP [2] algorithm. Here, the general methodology is to find pairs of corresponding features, between two scans and then align them as best as possible. Most methods utilize simple points, edges or plane features due to their ease of computation, but also more complex learned features have been proposed [14]. Regardless of used features, extracting them almost always involves the use of assumptions about the environment. While spatial subsampling strategies [4]

only make assumption about the expected scale of the environment, extracting planes and edges [15], [16], [17] additionally assume geometric properties such as planarity. To avoid making unnecessary or even incorrect assumption, we use a simple spatial subsampling strategy as proposed by [4].

Nearly all modern lidar odometry approaches utilize a filtering-based approach, where a new scan is registered to a local map derived from previous scans [4], [18], [19], [8]. The benefit of these methods is their speed with many of them achieving frame rates that far exceed the measurement frequency of the sensor. Their main problem is that they neglect the accumulation of error when constructing the map, which essentially leads to an increased amount of drift over long distances. SAM approaches try to counteract this by refining or updating the local map after a certain time. BALM [6] proposes the use of a joint optimization of the lidar scans inside the local window. A new scan is first aligned against a local map of plane and edge features to obtain an initial guess of the pose. Then the map is updated by inserting the features of the current lidar scan. After a certain number of insertions, a refinement is triggered which essentially aims at updating the poses inside the local window to better align the features of the local map. A similar method is presented in [20], where the authors assume indoor scenarios with an abundance of planes and walls. Because these methods optimize the map on a feature level, their computational complexity is proportional with the number of features in the map. In contrast, our proposed method circumnavigates this by optimizing higher level constraints instead of repeatedly aligning previous scans.

Other approaches that avoid the use of a feature based smoothing use point cloud registration methods to derive constraints for a pose graph optimization. This method was first used as a solution to the lidar SLAM method [9], [10], with the aim at aligning many lidar scans for an accurate and consistent map of the environment. In [9], the authors use a hierarchical graph approach that models groups of nodes of lower levels as one node at a higher level. This hierarchy decouples the optimization inside one graph of nodes from the optimization of another, which allows the authors to better direct the optimization to significant areas. A similar approach was taken in [10], where the authors used scan-to-scan matching to construct local maps of the area. After a certain amount of scans, the local maps are registered against each other, essentially leading to a double-stranded graph. A precise comparison between these methods and our approach is difficult as their aim is primarily to generate a consistent map and not to estimate the poses of the agent.

In the recent years, pose graph optimization has also been proposed for lidar odometry, mostly in the form of Lidar Inertial Odometry (LIO). Both [8] and [21] present an approach of integrating IMU and GNSS measurements. Lidar constraints from a scan-to-map registration are optimized together with constraints derived from other sensor modalities. One lidar-only pose graph based SAM approach is presented in [22]. By tracking features over multiple frames,

the authors are able to calculate multiple constraints from one alignment. When a new scan is registered, it is aligned against the local map which contains features, as well as the times at which the features were observed. By aligning a new scan, correspondences between features in the scan and features in the map are formed. The current scan may observe features from more than one previous scans, which allows the calculation of multiple individual constraints. Our approach is similar to this, as we also derive multiple constraints for one new lidar scan. However, our approach does not use a local map approach but instead uses multiple independent scan-to-scan registrations between the current scan and a set of previous keyframes, leading to a dense network of constraints which is beneficial in finding a locally consistent configuration of poses.

III. METHOD

Given a sequence of ego-centered lidar scans $\{\mathcal{P}_1, \dots, \mathcal{P}_t\}$ from a moving platform up to the current time t , the goal is to estimate the 6-DOF pose $\mathbf{x}_t \in \text{SE}(3)$ at the current time t . For the remainder of this paper we will adopt the following notation: States $\mathbf{x}_t \in \text{SE}(3)$ will be denoted by bold, lower case letters. Lidar scans, i.e., point clouds, will be denoted with calligraphic, upper case letters, e.g., \mathcal{P}_t . In both cases, a subscript indicates the time step. The superscript of a state \mathbf{x}_t^k indicates its reference frame. States without superscript are expressed in a global reference frame, and point clouds are always expressed in the ego-frame of the vehicle. Two subscripts divided by a colon denote a range. For example $\mathbf{X}_{i:t}$ denotes the range of poses between i and t .

The core idea of our method is to replace the classic single scan-to-map ICP registration with several individual scan-to-scan ICP registrations against a set of previously determined keyframes. Fig. 2 shows a detailed visualization of our method using a pose graph. The pose \mathbf{x}_7 of the newest scan is estimated by registering it against the previous keyframes inside a sliding window. These registrations, together with the registrations of previous time steps, form a network of constraints for a pose graph optimization.

Our proposed method can be divided into four modules. First, a preprocessing step that subsamples the raw point cloud via spatial subsampling. Second, an alignment step consisting of multiple scan-to-scan registration sub-steps, where the preprocessed point cloud is registered against a list of keyframes. In the third step, the relative transformations between the current scan and the keyframes are added as constraints to the pose graph optimization. The result of this step is a pose estimate for this time step and (optionally) a smoothed configuration of poses. The last step is the keyframe management that handles the insertion and deletion of keyframes.

A. Scan Preprocessing

For scan preprocessing we utilize a double voxel hash map approach as proposed by [4]. The raw data in the current time step t is first deskewed (if necessary) using the constant

motion model (1) and then inserted into a 3D voxel hash-map with a voxel size of $v_{\text{map}} = 0.5 \text{ m}$, keeping only the first inserted point per voxel. The result is a subset $\mathcal{K}_t \subseteq \mathcal{P}_t$ of the raw scan \mathcal{P}_t . \mathcal{K}_t is then subsampled a second time with an increased voxel size $v_{\text{ICP}} = 1.5 \text{ m}$, yielding $\mathcal{I}_t \subseteq \mathcal{K}_t \subseteq \mathcal{P}_t$. The stronger subsampled scan \mathcal{I}_t will be used for the registration and the denser \mathcal{K}_t will be used as a keyframe for future alignments with this scan.

B. Motion Prediction

Both speed and accuracy of the registration depend on the quality of the initialization. To this end, we utilize a simple constant motion model. Given the last two poses $\mathbf{x}_{t-1}, \mathbf{x}_{t-2} \in \text{SE}(3)$ in a global reference frame we can calculate the motion $\dot{\mathbf{x}}_{t-1} \in \text{SE}(3)$ of our platform at the last time step with

$$\dot{\mathbf{x}}_{t-1} = \mathbf{x}_{t-2}^{-1} \oplus \mathbf{x}_{t-1} \quad (1)$$

with \mathbf{x}^{-1} denoting the inverse transformation of \mathbf{x} and \oplus denoting the pose composition operator as described in [23]. Using the assumption of constant motion and constant time between frames we can calculate the predicted pose at the current time t with

$$\hat{\mathbf{x}}_t = \mathbf{x}_{t-1} \oplus \dot{\mathbf{x}}_{t-1} \quad (2)$$

C. Iterative Closest Point

In this section we will describe the ICP algorithm used for the scan registrations of our method. The application of the ICP algorithm between two point clouds \mathcal{A} and \mathcal{B} is denoted with

$$\Delta \mathbf{z}, \Omega = \text{ICP}(\mathcal{A}, \mathcal{B}) \quad (3)$$

The result $\Delta \mathbf{z} \in \text{SE}(3)$ is the transformation that aligns \mathcal{A} to \mathcal{B} and Ω will be used as the information matrix for the pose graph optimization in Section III-E. We use the Hessian method [24] as an approximation for the covariance of the registration but other more accurate methods could also be used [25].

The general implementation of ICP can be summarized as the repeated calculation of a set of correspondences $\mathcal{C} \subseteq \mathcal{A} \times \mathcal{B}$ followed by the minimization of the distances of these correspondences. These two steps are repeated until a local minimum is reached. For the calculation of correspondences we use a standard Nearest Neighbour (NN) search for all points $\mathbf{a} \in \mathcal{A}$ to any point $\mathbf{b} \in \mathcal{B}$ in a maximum search radius of $d_{\text{max}} = 3 \text{ m}$. Formally this can be written as

$$\mathcal{C} = \{(\mathbf{a}, \mathbf{b}) \mid \mathbf{a} \in \mathcal{A} \wedge \mathbf{b} = \underset{\mathbf{b}' \in \mathcal{B}}{\text{argmin}} \|\mathbf{a} - \mathbf{b}'\|_2 \wedge \|\mathbf{a} - \mathbf{b}\|_2 < d_{\text{max}}\} \quad (4)$$

For the optimization of the correspondences we use the Gauss-Newton method to minimize

$$\Delta \mathbf{z}_i = \underset{\mathbf{T} \in \text{SE}(3)}{\text{argmin}} \sum_{(\mathbf{a}, \mathbf{b}) \in \mathcal{C}_i} \rho(\|\mathbf{T}\mathbf{a} - \mathbf{b}\|_2) \quad (5)$$

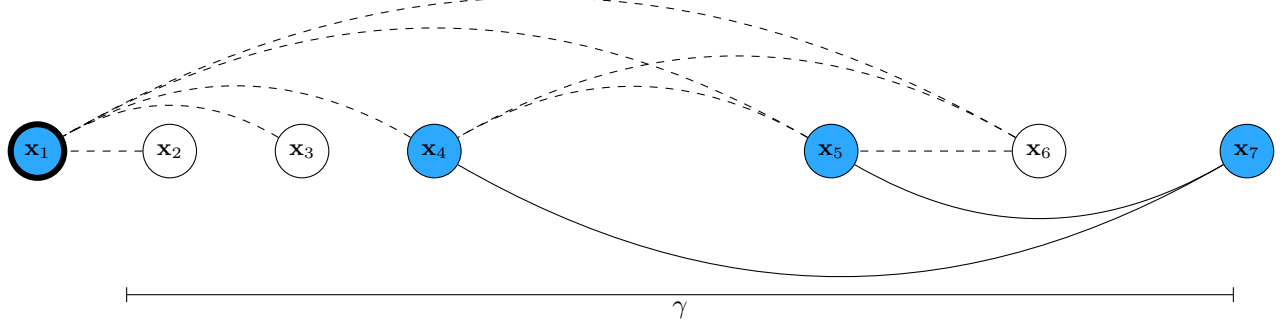


Fig. 2: Representation of the pose-graph constructed by our method. Blue nodes are the keyframes used for registration. A scan (\mathbf{x}_7) is registered against all previous keyframes inside the interval marked with γ . The constraints of previous time steps are displayed with dashed lines and constraints of the most recent time step are displayed as solid lines. The node \mathbf{x}_1 is outside the local window of \mathbf{x}_7 . It is not used for registration and its state is fixed.

with the subscript $(\cdot)_i$ indicating the iteration of the ICP algorithm. Instead of minimizing the squared distance, a robust kernel

$$\rho(e) = \frac{e^2/2}{\tau + e^2} , \quad (6)$$

as proposed in [26], is used to reduce the effect of outliers on the registration. Here, the parameter $\tau = 1/3\text{m}$ controls the distance beyond which correspondences are considered as outliers. Correspondence calculation and optimization are repeated until the convergence of $\Delta \mathbf{z}_i$, i.e., $\|\Delta \mathbf{z}_i\|_2 < 10^{-5}$. Between iterations \mathcal{A} is transformed with the last increment $\Delta \mathbf{z}_i$. The final result of the ICP algorithm is then the product of all increments computed as

$$\Delta \mathbf{z} = \Delta \mathbf{z}_N \oplus \Delta \mathbf{z}_{N-1} \oplus \dots \oplus \Delta \mathbf{z}_1 . \quad (7)$$

D. Multiple Scan-to-Scan Registration

Given a set of keyframes $\mathcal{R} = \{\mathcal{K}_{\alpha_1}, \dots, \mathcal{K}_{\alpha_N}\}$ from time steps $\{\alpha_1, \dots, \alpha_N\}$ with poses $\{\mathbf{x}_{\alpha_1}, \dots, \mathbf{x}_{\alpha_N}\}$, we register the current preprocessed lidar scan \mathcal{I}_t at the current time t independently to keyframes $\mathcal{K}_{\alpha_i} \in \mathcal{R}$. The predicted pose $\hat{\mathbf{x}}_t$ from our motion model (2) is first expressed in the reference frame of the keyframe under consideration \mathcal{K}_{α_i} with

$$\hat{\mathbf{x}}_t^{\alpha_i} = \mathbf{x}_{\alpha_i}^{-1} \oplus \hat{\mathbf{x}}_t . \quad (8)$$

The result $\hat{\mathbf{x}}_t^{\alpha_i}$ is used as an initial guess for an ICP registration between the current scan \mathcal{I}_t and the keyframe \mathcal{K}_{α_i}

$$\Delta \mathbf{z}_t^{\alpha_i}, \Omega_t^{\alpha_i} = \text{ICP}(\hat{\mathbf{x}}_t^{\alpha_i} \cdot \mathcal{I}_t, \mathcal{K}_{\alpha_i}) , \quad (9)$$

resulting in a correction $\Delta \mathbf{z}_t^{\alpha_i}$ of the initial guess $\hat{\mathbf{x}}_t^{\alpha_i}$, as well as the corresponding information matrix $\Omega_t^{\alpha_i}$. The product operator $(\cdot) : \text{SE}(3) \times \mathbb{R}^{N \times 3} \rightarrow \mathbb{R}^{N \times 3}$ indicates the element-wise application of a transformation to all points of a point cloud. The corrected (relative) pose $\mathbf{z}_t^{\alpha_i}$ of this registration can then be obtained with

$$\mathbf{z}_t^{\alpha_i} = \Delta \mathbf{z}_t^{\alpha_i} \oplus \hat{\mathbf{x}}_t^{\alpha_i} . \quad (10)$$

This procedure is applied for all keyframes, resulting in a set of pose-information tuples $\mathcal{C}_t = \{(\mathbf{z}_t^{\alpha_1}, \Omega_t^{\alpha_1}), \dots, (\mathbf{z}_t^{\alpha_N}, \Omega_t^{\alpha_N})\}$ which will be added to the pose graph optimization as the constraints of the current time step.

To increase performance and avoid the registration of two scans that only have a minimal overlap, we additionally check for a minimum number of correspondences when registering two lidar scans. If the number of correspondences at any iteration of the registration process is lower than some threshold, the registration is canceled and discarded from \mathcal{C}_t . This ensures that the graph only contains meaningful constraints. We set the minimum number of correspondences to 200.

Fig. 2 is a visualization of the pose graph constructed by our method. The constraints computed during this time step are shown in solid lines and the constraints from previous time steps are shown in dashed. The current frame \mathbf{x}_7 is aligned against the previous keyframes \mathbf{x}_4 and \mathbf{x}_5 . The keyframe \mathbf{x}_1 is already too far away and therefore not considered for the registration.

E. Smoothing via Pose Graph Optimization

The pose graph optimization step takes a set of constraints $\mathcal{C}_{\alpha_i:t} = \mathcal{C}_{\alpha_i} \cup \mathcal{C}_{\alpha_i+1} \cup \dots \cup \mathcal{C}_t$ as well as an initial configuration of poses $\mathbf{X}_{\alpha_i:t} = \{\mathbf{x}_{\alpha_i}, \mathbf{x}_{\alpha_i+1}, \dots, \mathbf{x}_t\}$ as input and returns an updated configuration of poses $\mathbf{X}_{\alpha_i:t}^* = \{\mathbf{x}_{\alpha_i}^*, \mathbf{x}_{\alpha_i+1}^*, \dots, \mathbf{x}_t^*\}$ that better satisfies the constraints. The constraints $\mathcal{C}_{\alpha_i:t-1}$ and initial poses $\mathbf{X}_{\alpha_i:t-1}$ are known from the previous time step and the constraints of the current time steps \mathcal{C}_t are computed as explained in Section III-D. For the initial guess of the state of the current time step \mathbf{x}_t we use the registration result of the last keyframe with the current scan expressed in the global reference frame $\mathbf{z}_t^{\alpha_N} \oplus \mathbf{x}_{\alpha_N}$.

The error function

$$\mathbf{e}(\mathbf{x}_i, \mathbf{x}_j, \mathbf{z}_i^j) = (\mathbf{z}_i^j)^{-1} \oplus (\mathbf{x}_j^{-1} \oplus \mathbf{x}_i) \quad (11)$$

computes the distance from the measurement \mathbf{z}_i^j , obtained from the registration of scan i to scan j , to the expected

measurement between the poses \mathbf{x}_i and \mathbf{x}_j . For brevity and consistency with standard pose graph notation, we shorten (11) as well as notation for the information matrices Ω_i^j and measurements \mathbf{z}_i^j with

$$\mathbf{e}_{ij} \stackrel{\text{def}}{=} \mathbf{e}(\mathbf{x}_i, \mathbf{x}_j, \mathbf{z}_i^j), \quad (12)$$

$$\Omega_{ij} \stackrel{\text{def}}{=} \Omega_i^j, \quad (13)$$

$$\mathbf{z}_{ij} \stackrel{\text{def}}{=} \mathbf{z}_i^j. \quad (14)$$

The calculation of the best configuration of poses $\mathbf{X}_{\alpha_i:t}^*$ can then be written as the minimization problem

$$\mathbf{X}_{\alpha_i:t}^* = \underset{\mathbf{X}}{\operatorname{argmin}} \sum_{(\mathbf{z}_{ij}, \Omega_{ij}) \in \mathcal{C}_{\alpha_i:t}} \mathbf{e}_{ij}^T \Omega_{ij} \mathbf{e}_{ij}. \quad (15)$$

We skip a detailed discussion of problems and difficulties of pose graph optimization in 3D and instead refer the interested reader to [9], [27]. Since the set of constraints $\mathcal{C}_{(\alpha_i:t)}$ largely remains the same between time steps, we have found an small number of 15 iterations of the Levenberg–Marquardt algorithm to yield good results when optimizing (15). For the implementation of pose graph optimization we have used the g2o library¹.

F. Keyframe Management

The final task in our pipeline is the insertion and deletion of keyframes. First, the states $\mathbf{X}_{\alpha_i:t}$ used as the initial estimates for the pose graph optimization are updated with the optimized configuration $\mathbf{X}_{\alpha_i:t}^*$ obtained from (15). Again, let $\mathcal{K} = \{\mathcal{K}_{\alpha_1}, \dots, \mathcal{K}_{\alpha_N}\}$ be the current list of keyframes at time steps $\{\alpha_1, \dots, \alpha_N\}$ with the corresponding (updated) poses $\{\mathbf{x}_{\alpha_1}, \dots, \mathbf{x}_{\alpha_N}\}$. The current scan \mathcal{K}_t is appended to the list of keyframes \mathcal{K} if the distance between the current pose \mathbf{x}_t and the pose of the last keyframe \mathcal{K}_{α_N} exceeds a limit of $\kappa = 3\text{m}$. Likewise, all keyframes \mathcal{K}_{α_i} are removed from the list of keyframes, if their distance to the current pose \mathbf{x}_t exceeds another threshold γ . We found a value for γ of one third of the maximum distance of the lidar to generally give good results and therefore used it through the experiments.

IV. EVALUATION

We have conducted experiments on three different real-world lidar odometry datasets to judge the performance of our system. On all datasets we have used the same configuration of parameters, with the exception of γ , which was set according to a third of the maximum lidar distance of 100m, 120m and 160m for the KITTI [11], MulRan [12] and our own dataset [28], respectively. The Relative Translational Error (RTE) metric, as reported on the KITTI odometry leaderboard², was used for the evaluation. For the comparison we have included the three publicly available state-of-the-art lidar odometry methods MAD-ICP [18], KISS-ICP [4] and CT-ICP [29]. Due to incompatibilities we were not able to evaluate CT-ICP on our custom dataset. On the KITTI dataset we additionally included the results of [22],

TABLE I: Results of our method on different data sets. Best results are indicated in **bold**.

		MAD-ICP [18]	KISS-ICP [4]	CT-ICP [29]	[22]	Ours
KITTI	0	0.73	0.51	0.50	0.53	0.70
	1	0.85	0.72	0.67	0.77	0.84
	2	0.76	0.53	0.51	0.52	0.61
	3	0.84	0.66	0.70	0.65	0.94
	4	0.69	0.35	0.35	0.38	0.42
	5	0.48	0.30	0.26	0.30	0.44
	6	0.48	0.26	0.28	0.34	0.33
	7	0.45	0.33	0.32	0.33	0.46
	8	1.21	0.82	0.81	0.82	1.01
	9	1.02	0.49	0.48	0.49	0.65
	10	0.96	0.56	0.52	0.55	0.73
	avg	0.82	0.54	0.53	0.55	0.69
MulRan	DCC01	3.06	2.95	4.91		2.65
	DCC02	2.28	2.50	4.18		2.09
	DCC03	1.92	2.11	4.63		1.73
	KAIST01	2.36	2.36	4.33		2.07
	KAIST02	2.32	2.31	4.02		2.07
	KAIST03	2.74	2.68	4.60		2.40
	River.01	3.77	3.55	7.08		3.34
	River.02	3.46	3.34	6.20		3.10
	River.03	2.48	2.51	5.78		2.13
	Sejong01	4.54	4.40	9.08		3.88
	Sejong02	6.21	4.82	4.14		4.33
	Sejong03	6.33	5.03	4.90		8.77
	avg	4.34	3.82	6.25		4.12
Ours [28]	r1	0.75	0.69			0.57
	r2	0.71	0.62			0.56
	r3	0.73	0.65			0.61
	b4	0.74	0.60			0.62
	b5	0.82	0.67			0.66
	avg	0.78	0.64			0.63

another lidar-only smoothing and mapping approach. Results are shown in Table I.

A. KITTI

On the KITTI dataset, our approach performs slightly better than MAD-ICP but worse than the other methods. In general, all methods perform well on this dataset, with the performance of KISS-ICP, CT-ICP and [22] being almost equal. We found the motion of the vehicle to sometimes not coincide with the observed lidar scans. This aligns with the poor local consistency reported by [18] and, since the smoothing step of our method aims at providing a consistent set of poses, might be a reason for the comparably bad performance of our method.

B. MulRan

On the MulRan dataset, our method performed significantly better than the all other competitors on 11 out of the 12 sequences. However, our method experienced problems when traversing tunnels, which increased the error on the Sejong03 sequence, in turn also increasing the overall average error by a large margin. The problem in such scenarios is the featureless environment which make consecutive lidar scans look identical from the point-of-view of the sensor, making

¹<https://github.com/RainerKuemmerle/g2o>

²https://www.cvlibs.net/datasets/kitti/eval_odometry.php

a registration unstable. This caused a large rotational error near the end of the tunnel, increasing the mean error on this trajectory drastically. Overall, KISS-ICP performed best, but when excluding the outlier sequence Sejong03, our method ranks first with an error of 2.34, followed by KISS-ICP with an error of 2.90, an improvement of around 20%.

C. Custom Dataset

Our custom dataset features 5 drives on three different trajectories in urban and suburban areas in Germany. As a lidar sensor, an Ouster OS1-128 rev.7 operated at 20Hz was used. More information about the dataset can be found in our previous work [28]. Our method outperforms MAD-ICP on all and KISS-ICP on all but one sequence of the dataset. Overall, our method is slightly better than KISS-ICP.

V. CONCLUSION

In this paper we have motivated and presented a lidar-only odometry approach with real-time filtering and lagged smoothing capabilities. At every time step, the current lidar scan is registered independently against a set of previous keyframes, yielding a new set of constraints for a pose graph optimization. Together with the constraints of the previous time step we are able to produce an accurate estimate for the current time step as well as a consistent set of previous poses. The proposed method yields comparable results to other state-of-the-art methods on the KITTI and our own dataset and significantly outperforms them on a majority of the MulRan dataset. A direction of further research should be the robustification of our method to avoid divergence as seen on the MulRan dataset. Here, the use of additional motion constraints or a more complex feature extraction could be explored. Furthermore, the integration of IMU measurements could be a possibility, due to the native ability of the graph-based approach to account for such additional information.

REFERENCES

- [1] S. A. Mohamed, M.-H. Haghbayan, T. Westerlund, J. Heikkinen, H. Tenhunen, and J. Plosila, "A survey on odometry for autonomous navigation systems," *IEEE Access*, vol. 7, pp. 97 466–97 486, 2019.
- [2] P. J. Besl and N. D. McKay, "Method for registration of 3-D shapes," in *Sensor fusion IV: control paradigms and data structures*, vol. 1611. Spie, 1992, pp. 586–606.
- [3] F. Pomerleau, F. Colas, R. Siegwart, and S. Magnenat, "Comparing ICP variants on real-world data sets: Open-source library and experimental protocol," *Autonomous robots*, vol. 34, pp. 133–148, 2013.
- [4] I. Vizzo, T. Guadagnino, B. Mersch, L. Wiesmann, J. Behley, and C. Stachniss, "KISS-ICP: In defense of point-to-point ICP – simple, accurate, and robust registration if done the right way," *IEEE Robotics and Automation Letters (RA-L)*, vol. 8, no. 2, pp. 1029–1036, 2023.
- [5] M. Kaess, A. Ranganathan, and F. Dellaert, "iSAM: Incremental smoothing and mapping," *IEEE Transactions on Robotics*, vol. 24, no. 6, pp. 1365–1378, 2008.
- [6] Z. Liu and F. Zhang, "BALM: Bundle adjustment for lidar mapping," *IEEE Robotics and Automation Letters*, vol. 6, no. 2, pp. 3184–3191, 2021.
- [7] S. Liang, Z. Cao, J. Yu, M. Tan, and S. Wang, "A tight filtering and smoothing fusion method with feature tracking for lidar odometry," *IEEE Sensors Journal*, vol. 22, no. 13, pp. 13 622–13 631, 2022.
- [8] T. Shan, B. Englot, D. Meyers, W. Wang, C. Ratti, and R. Daniela, "LIO-SAM: Tightly-coupled lidar inertial odometry via smoothing and mapping," in *IEEE/RSJ International Conference on Intelligent Robots and Systems (IROS)*. IEEE, 2020, pp. 5135–5142.
- [9] G. Grisetti, R. Kümmerle, C. Stachniss, U. Frese, and C. Hertzberg, "Hierarchical optimization on manifolds for online 2D and 3D mapping," in *2010 IEEE International Conference on Robotics and Automation*. IEEE, 2010, pp. 273–278.
- [10] D. Droschel and S. Behnke, "Efficient continuous-time SLAM for 3D lidar-based online mapping," in *2018 IEEE International Conference on Robotics and Automation (ICRA)*. IEEE, 2018, pp. 5000–5007.
- [11] A. Geiger, P. Lenz, and R. Urtasun, "Are we ready for autonomous driving? The KITTI vision benchmark suite," in *2012 IEEE conference on computer vision and pattern recognition*. IEEE, 2012, pp. 3354–3361.
- [12] G. Kim, Y. S. Park, Y. Cho, J. Jeong, and A. Kim, "MulRan: Multimodal range dataset for urban place recognition," in *2020 IEEE international conference on robotics and automation (ICRA)*. IEEE, 2020, pp. 6246–6253.
- [13] P. Biber and W. Straßer, "The normal distributions transform: A new approach to laser scan matching," in *Proceedings 2003 IEEE/RSJ International Conference on Intelligent Robots and Systems (IROS 2003)(Cat. No. 03CH37453)*, vol. 3. IEEE, 2003, pp. 2743–2748.
- [14] Y. He and C.-H. Lee, "An improved ICP registration algorithm by combining PointNet++ and ICP algorithm," in *2020 6th International Conference on Control, Automation and Robotics (ICCAR)*. IEEE, 2020, pp. 741–745.
- [15] J. Zhang and S. Singh, "LOAM: Lidar odometry and mapping in real-time," in *Robotics: Science and systems*, vol. 2, no. 9. Berkeley, CA, 2014, pp. 1–9.
- [16] J.-E. Deschaud, "IMLS-SLAM: Scan-to-model matching based on 3D data," in *2018 IEEE International Conference on Robotics and Automation (ICRA)*. IEEE, 2018, pp. 2480–2485.
- [17] Y. Pan, P. Xiao, Y. He, Z. Shao, and Z. Li, "MULLS: Versatile lidar SLAM via multi-metric linear least square," in *2021 IEEE International Conference on Robotics and Automation (ICRA)*. IEEE, 2021, pp. 11 633–11 640.
- [18] S. Ferrari, L. Di Giammarino, L. Brizi, and G. Grisetti, "MAD-ICP: It is all about matching data-robust and informed lidar odometry," *IEEE Robotics and Automation Letters*, 2024.
- [19] T. Shan and B. Englot, "LeGO-LOAM: Lightweight and ground-optimized lidar odometry and mapping on variable terrain," *2018 IEEE/RSJ International Conference on Intelligent Robots and Systems (IROS)*, pp. 4758–4765, 2018.
- [20] L. Zhou, D. Koppel, and M. Kaess, "Lidar SLAM with plane adjustment for indoor environment," *IEEE Robotics and Automation Letters*, vol. 6, no. 4, pp. 7073–7080, 2021.
- [21] H. Ye, Y. Chen, and M. Liu, "Tightly coupled 3D lidar inertial odometry and mapping," in *2019 International Conference on Robotics and Automation (ICRA)*. IEEE, 2019, pp. 3144–3150.
- [22] S. Liang, Z. Cao, C. Wang, and J. Yu, "Hierarchical estimation-based lidar odometry with scan-to-map matching and fixed-lag smoothing," *IEEE Transactions on Intelligent Vehicles*, vol. 8, no. 2, pp. 1607–1623, 2022.
- [23] J. L. Blanco-Claraco, "A tutorial on SE(3) transformation parameterizations and on-manifold optimization," *arXiv preprint arXiv:2103.15980*, 2021.
- [24] O. Bengtsson and A.-J. Baerveldt, "Robot localization based on scan-matching—estimating the covariance matrix for the IDC algorithm," *Robotics and Autonomous Systems*, vol. 44, no. 1, pp. 29–40, 2003.
- [25] A. Censi, "An accurate closed-form estimate of ICP's covariance," in *Proceedings 2007 IEEE International Conference on Robotics and Automation*. IEEE, 2007, pp. 3167–3172.
- [26] N. Chebrolu, T. Läbe, O. Vysotska, J. Behley, and C. Stachniss, "Adaptive robust kernels for non-linear least squares problems," *IEEE Robotics and Automation Letters*, vol. 6, no. 2, pp. 2240–2247, 2021.
- [27] G. Grisetti, R. Kümmerle, C. Stachniss, and W. Burgard, "A tutorial on graph-based SLAM," *IEEE Intelligent Transportation Systems Magazine*, vol. 2, no. 4, pp. 31–43, 2010.
- [28] A. Kurda, S. Steuernagel, L. Jung, and M. Baum, "Reducing drift of lidar odometry by incorporating OpenStreetMap building data," Sept. 2024. [Online]. Available: <http://dx.doi.org/10.36227/techrxiv.172349303.35859650/v2>
- [29] P. Dellenbach, J.-E. Deschaud, B. Jacquet, and F. Goulette, "CT-ICP: Real-time elastic lidar odometry with loop closure," in *2022 International Conference on Robotics and Automation (ICRA)*. IEEE, 2022, pp. 5580–5586.